01,05

Control of a SOT-MRAM Cell by External Magnetic Field and Current

© N.V. Ostrovskaya, V.A. Skidanov, Yu.A. Yusipova

Institute for Design Problems in Microelectronics of the Russian Academy of Sciences, Zelenograd, Moscow, Russia

E-mail: ost.ippm@yandex.ru

Received April 18, 2024
Revised April 18, 2024
Accepted May 8, 2024

A dynamic system has been constructed that describes the dynamics of magnetization in a magnetic random-access memory element based on the spin Hall effect. The configuration of a cell with perpendicular anisotropy of the active layer and the dynamics of magnetization in the layer under the influence of charge-current pulses and an external magnetic field are considered. A qualitative analysis of the dynamic system was carried out. The equilibrium states of the system are identified and a classification of the main dynamic modes is carried out. The critical value of the switching current is calculated.

Keywords: spintronics, orbitronics, magnetization, Landau–Lifshitz–Hilbert equation, spin Hall effect, spin current, charge current, spin torque.

DOI: 10.61011/PSS.2024.06.58686.31HH

1. Introduction

Spin-polarized current, which allows the transfer of spin angular momentum between two magnetic layers is a main option to control the states of bits in magnetic memory, called STT-MRAM [1–3]. SOT-MRAM memory is an alternative to such memory, which has the properties of non-volatility, reversibility, high speed, low power dissipation and good compatibility with the traditional semiconductor industry. Several configurations of SOT-MRAM cells with different properties are currently proposed [4]. The dynamics of magnetization in the active layer of cells with perpendicular anisotropy based on the spin Hall effect is studied in this paper.

2. Basic equations

The description of the dynamics of the magnetization vector of the free layer $\mathbf{M}$ is based on the Landau–Lifshitz–Gilbert equation (LLG):

$$\frac{\partial \mathbf{M}}{\partial t} = -\gamma\mu_0[\mathbf{M}\times\mathbf{H}_{\text{eff}}] + \frac{\alpha}{M_s}\left[\mathbf{M}\times\frac{\partial \mathbf{M}}{\partial t}\right] + \mathbf{T}_{\text{SOT}}, \quad (1)$$

where the spin-orbit toque $\mathbf{T}_{\text{SOT}}$ is equal to

$$\mathbf{T}_{\text{SOT}} = \mathbf{T}_{\text{FL}} + \mathbf{T}_{\text{DL}}$$

$$= \gamma\mu_0 j\theta_{\text{SH}}\chi_{\text{DL}}[\mathbf{M}\times[\mathbf{M}\times\mathbf{e}_y]] + \gamma\mu_0 j\theta_{\text{SH}}\chi_{\text{FL}}M_s[\mathbf{M}\times\mathbf{e}_y].$$

Here γ — gyromagnetic ratio; μ_0 — magnetic permeability of vacuum; $\mathbf{H}_{\text{eff}}$ — effective magnetic field; α — dimensionless dissipation coefficient; j — normalized charge current density, $j = J/J_{\text{norm}} = J\hbar/(g|e|d\mu_0 M_s^2)$; $\hbar$ — Planck's constant; $g \simeq 2$ — Lande factor; e — electron charge; d — thickness of the free ferromagnetic layer; M_s — saturation magnetization of the free (active) ferromagnetic layer (the values of the parameters of the three-layer structure $Ta|Co_{60}Fe_{20}B_{20}|MgO$ used in the article are given in Table 1); $\theta_{\text{SH}} = j_s/j_c$ — the angle of the spin Hall effect characterizing the ratio of the density of the vertical spin current j_s to the density of the horizontal charge current j_c; $\chi_{\text{DL}}, \chi_{\text{FL}}$ — the efficiency of the spin Hall effect for each component of the torque.

Figure 1 shows a scheme of the considered model. On the basis of analogy with the models considered in [5], we call this cell configuration the YZ model (the external magnetic field is directed along the Y axis, the anisotropy field — along the Z axis, orthogonal to the plane of the layer).

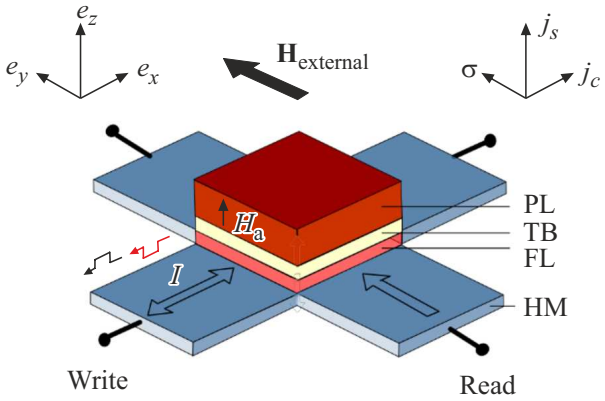

Figure 1. Schematic representation of the SOT-MRAM element with perpendicular anisotropy of ferromagnetic layers ($\mathbf{H}_{\text{external}}$ — external magnetic field, $\mathbf{H}_a$ — anisotropy field, I — charging recording current, $\mathbf{j}_c$ — charge current density vector, $\mathbf{j}_s$ — spin current density vector, $\boldsymbol{\sigma}$ — spin polarization direction). PL — pinned layer, FL — free layer, TB — tunnel barrier, HM — heavy metal.

Table 1. Parameters for modeling the dynamics of the SOT-MRAM element for the Ta|$Co_{60}Fe_{20}B_{20}$|MgO ferromagnet

Physical Quantity	Numerical Value	Link
K, MJ/m^3	0.6	[6]
$\mu_0 M_s$,T	1.300	[6]
α	0.008	[7]
θ_{SH}	−0.06	[4]
χ_{DL}	3.2	[4]
χ_{FL}	−2.1	[4]
$k = 2K/(\mu_0 M_s^2)$	0.892	–

Table 2. The normalizations used in the calculations (the thickness of the active layer d is 1 nm, the Lande factor g is considered equal to 2)

The normalization formula	Normalization factor
$H = hM_s$, MA/m	$1.035 \cdot 10^6 h$
$J = dge\mu_0 jM_s^2/\hbar$, A/m^2	$4.081 \cdot 10^{12} j$
$K = \mu_0 M_s^2 k/2$, J/m^3	$6.724 \cdot 10^5 k$
$t = \tau(1+\alpha^2)/(\gamma\mu_0 M_s)$, s	$2.745 \cdot 10^{-11}\tau$

The normalization values for the above values are listed in Table 2 ([4]).

Let us present equation (1) in a dimensionless form to use the apparatus of numerical analysis

$$\frac{\partial \mathbf{m}}{\partial \tilde{\tau}} = -\mathbf{m} \times \mathbf{h}_{\text{eff}} + \alpha \mathbf{m} \times \frac{\partial \mathbf{m}}{\partial \tilde{\tau}} + \mathbf{t}, \qquad (3)$$

where

$$\mathbf{m} = \frac{\mathbf{M}}{M_s}(|\mathbf{m}| = 1),\ \mathbf{h}_{\text{eff}} = \frac{\mathbf{H}_{\text{eff}}}{M_s},\ \mathbf{t} = \frac{\mathbf{T}}{\gamma\mu_0 M_s^2},\ \tilde{\tau} = \gamma\mu_0 M_s^2 t.$$

Let's assume that the active layer of the memory element SOT-MRAM is a Stoner–Wohlfarth particle, i. e. the exchange interaction in the model can be ignored. Let us assume that the effective field in the model consists of three components: an external magnetic field $\mathbf{h}_{\text{external}} = h\mathbf{e}_y$, an anisotropy field directed perpendicular to the plane of the cross section of the memory element $\mathbf{h}_{\text{anisotropy}} = k(\mathbf{m}, \mathbf{e}_z)\mathbf{e}_z$, ($k = 2K_a\mu_0^{-1}M_s^{-2}$ — material quality factor, K_a — anisotropy constant), and demagnetization fields $\mathbf{h}_{\text{demanetization}} = -\hat{\mathbf{q}}\mathbf{m}$, where tensor $\hat{\mathbf{q}}$ — demagnetization factor. It is possible to assume in the simplest case of a square cross-section MRAM cell that the tensor $\hat{\mathbf{q}}$ has only one nonzero element on the main diagonal, close in magnitude to one, $q_{33} = 1$ [12,13]. If this amount is replenished with the effective field created by the spin-orbit interaction, then the new effective field will be equal to

$$\mathbf{f}_{\text{eff}} = \mathbf{h}_{\text{external}} + \mathbf{h}_{\text{anisotropy}} + \mathbf{h}_{\text{demanetization}} + \mathbf{h}_{\text{DL}} + \mathbf{h}_{\text{FL}}. \quad (4)$$

The coordinate representation of the effective field is (4) has the following form in the case of a magnetic field applied along the Y axis

$$\mathbf{f}_{\text{eff}} = (f_x, f_y, f_z)^{\text{T}} = (bjm_z, h - cj, (k-1)m_z - bjm_x)^{\text{T}},$$

where $b = \theta_{SH}\chi_{DL}$, $c = \theta_{SH}\chi_{FL}$.

We obtain the following by solving the equation (3) with respect to the time derivative

$$\frac{\partial \mathbf{m}}{\partial \tau} = -\mathbf{m} \times \mathbf{f}_{\text{eff}} + \alpha \mathbf{f}_{\text{eff}}(\mathbf{m}, \mathbf{m}) - \alpha \mathbf{m}(\mathbf{m}, \mathbf{f}_{\text{eff}}), \qquad (5)$$

where

$$\tau = \frac{\tilde{\tau}}{1+\alpha^2} = |\gamma|\frac{\mu_0 M_s}{1+\alpha^2}t,\ (\mathbf{m}, \mathbf{m}) = 1.$$

The transition from the equation (3) to the equation (5) is provided in Appendix. Therefore, the equation (5) has the following form in the coordinate notation

$$\frac{dm_x}{d\tau} = (m_z f_y - m_y f_z) + \alpha f_x - \alpha m_x L,$$

$$\frac{dm_y}{d\tau} = (m_x f_z - m_z f_x) + \alpha f_y - \alpha m_y L,$$

$$\frac{dm_z}{d\tau} = (m_y f_x - m_x f_y) + \alpha f_z - \alpha m_z L,$$

where $L = (\mathbf{m}, \mathbf{f}) = (h - c_j)m_y + (k-1)m_z^2$. And finally, a dynamic system is obtained for the considered model

$$\begin{aligned}
\frac{dm_x}{d\tau} &= (h - cj + \alpha bj)m_z - (k-1)m_y m_z \\
&\quad + (bj + \alpha cj - \alpha h)m_x m_y - \alpha(k-1)m_x m_z^2, \\
\frac{dm_y}{d\tau} &= (k-1)m_x m_z + (\alpha h - \alpha cj - bj)(m_x^2 + m_z^2) \\
&\quad - \alpha(k-1)m_y m_z^2, \\
\frac{dm_z}{d\tau} &= -(h - cj + \alpha bj)m_x + \alpha(k-1)m_z \\
&\quad + (bj - \alpha h + \alpha cj)m_y m_z - \alpha(k-1)m_z^3. \qquad (6)
\end{aligned}$$

The phase surface for the dynamical system (6) is the surface of a unit sphere (Poincare-Bloch sphere). One and only one phase trajectory passes through a regular point on the phase surface. If a point is special, then, according to Cauchy's theorem, the phase trajectory at this point either does not exist, or the uniqueness condition is violated in it. This allows determining the number and coordinates of singular points, which, in turn, allows classifying possible types of dynamics of variables in a dynamic system.

3. Dynamic system analysis

Let us denote some selected points of the system in coordinates $(\mathbf{e}_x, \mathbf{e}_y, \mathbf{e}_z)$ as $T_{1,2}(\mp 1, 0, 0)$, $T_{3,4}(0, \mp 1, 0)$, $T_{5,6}(0, 0, \mp 1)$.

It follows from (6) that there are always at least two singular points, $T_{3,4}(0, \mp 1, 0)$ in the Y-model, which we will call the main ones. The type of singular points is determined by the Jacobian eigenvalues

$$D = \begin{pmatrix} \partial P/\partial m_x & \partial P/\partial m_y & \partial P/\partial m_z \\ \partial Q/\partial m_x & \partial Q/\partial m_y & \partial Q/\partial m_z \\ \partial S/\partial m_x & \partial S/\partial m_y & \partial S/\partial m_z \end{pmatrix}, \qquad (7)$$

where P, Q, S — the right parts of the dynamic system (6).

3.1. Singular point $T_4(0, +1, 0)$

Jacobian (7) at the singular point $T_4(0, +1, 0)$ is equal to

$$D_1 = \begin{pmatrix} -\alpha h + (b + \alpha c) j & 0 & h - (\alpha b - c) j + (1 - k) \\ 0 & -2\alpha(h - cj) & 0 \\ -h - (\alpha b - c) j & 0 & -\alpha h + (b + \alpha c) j - \alpha(1 - k) \end{pmatrix}.$$

The Jacobian eigenvalues at this point are

$$\lambda_{1,2} = bj + \alpha(cj - h) + \frac{1}{2}\alpha(k - 1)$$

$$\pm \sqrt{\begin{array}{l} -[2(h - cj + \alpha bj) - (k - 1)(\sqrt{\alpha^2 + 1} + 1)] \\ \times [2(h - cj + \alpha bj) + (k - 1)(\sqrt{\alpha^2 + 1}) - 1)] \end{array}},$$

$$\lambda_3 = -2\alpha(h - cj). \qquad (9)$$

Since (6) is a system with two degrees of freedom, the type of singular point can be defined as the type of singular point on the projection of its neighborhood onto a plane tangent to the unit sphere at the singular point. That is, two eigenvalues are sufficient to determine the type of a singular point. In particular, the focus can be determined by whether $\lambda_{1,2}$ are valid or complex conjugate, depending on the sign of the root expressions in (8). Since the subcortical expression splits into the product of two linear expressions with respect to variables h, j, then the region on the plane (h, j) in which it is positive is bounded by two parallel lines (Figure 2, *a*):

$$L_1: \; 2h + 2(\alpha b - c) j - (k - 1)(\sqrt{\alpha^2 + 1} + 1) = 0,$$

$$L_2: \; 2h + 2(\alpha b - c) j + (k - 1)(\sqrt{\alpha^2 + 1} - 1) = 0. \quad (9a)$$

The lines L_1 and L_2 intersect the axis h at points

$$h_1 = \frac{1}{2}(k - 1)(\sqrt{\alpha^2 + 1} + 1) \approx k - 1)(1 + O(\alpha)),$$

$$h_2 \approx \frac{1}{4}\alpha(k - 1) = O(\alpha).$$

If the root expressions in (8) are positive, then the singular point can be a node or a saddle, which can be determined by the sign of the product of the eigenvalues $\lambda_1\lambda_2$ — the product is positive for a node type point (both stable and unstable), and it is negative in case of a saddle. Therefore, the point $T_4(0, +1, 0)$ is a node or saddle in the band between the lines L_1 and L_2, it is a focus outside the band. The boundary between the regions where the singular point is a saddle or node runs along a second-order line

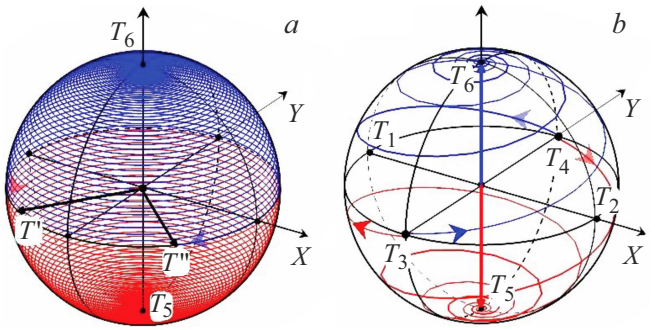

Figure 2. Dynamics of the magnetization vector at $h = 0$, $j = 0$: *a* — $k < 1$, *b* — $k > 1$.

$$L_3: \; (b^2 + c^2) j^2 - 2chj - (1 - k) cj + h^2 + (1 - k) h = 0, \qquad (10)$$

its canonical equation is the ellipse equation

$$\frac{u^2}{p^2} + \frac{v^2}{s^2} = 1,$$

where

$$p^2 = 2\frac{c^2 + b^2 + 1 - d}{(k - 1)^2}, \quad s^2 = 2\frac{c^2 + b^2 + 1 + d}{(k - 1)^2},$$

$$d = \sqrt{(c^2 + b^2 + 21)^2 - 4b^2}, \quad u = h - (k - 1), \quad v \equiv j.$$

The ellipse is rotated relative to the coordinate axes on the plane „field–current“ by angle

$$\varphi = \frac{1}{2}\,\mathrm{arctg}\,\frac{2c}{b^2 + c^2 - 1}$$

and shifted relative to the origin along the horizontal axis h by $k - 1$. The lines L_1 and L_2 touch the ellipse (10) at points $S_1(h_1, j_1)$ and $S_2(h_2, j_2)$, where

$$h_1 = (k - 1)\frac{(b + \alpha c) + b\sqrt{1 + \alpha^2}}{2b\sqrt{1 + \alpha^2}}, \; j_1 = \frac{\alpha(k - 1)}{2b\sqrt{1 + \alpha^2}},$$

$$h_2 = (k - 1)\frac{(b - \alpha c) - b\sqrt{1 + \alpha^2}}{2b\sqrt{1 + \alpha^2}}, \; j_2 = \frac{\alpha(k - 1)}{2b\sqrt{1 + \alpha^2}},$$

It should be also noted that in the case where the point $T_4(0, +1, 0)$ is the focus, according to the Andronov-Hopf theorem, the line L_4

$$L4: \; -2\alpha h + 2(b + ac) j + \alpha(1 - k) = 0 \qquad (11)$$

is a line of birth/disappearance of limit cycles. The line separates the regions where there are limit cycles around the point $T_4(0, +1, 0)$ and the regions where there are no limit cycles (Figure 2, *a*). This line crosses the points $S_1(h_1, j_1)$ and $S_2(h_2, j_2)$.

3.2. Singular point $T_3(0, -1, 0)$

Similarly, at the singular point $T_3(0, -1, 0)$, the eigenvalues of the Jacobian are equal to

$$\lambda_{1,2} = -bj - \alpha(cj - h) + \frac{1}{2}\alpha(k-1) \pm \sqrt{\begin{array}{l}-[2(h - cj + \alpha bj) - (k-1)(\sqrt{\alpha^2+1} - 1)] \\ \times[2(h - cj + \alpha bj) + (k-1)(\sqrt{\alpha^2+1}) + 1)]\end{array}},$$
$$\lambda_3 = 2\alpha(h - cj). \quad (12)$$

The region of real eigenvalues is bounded by straight lines in this case

$$L_1': \ 2h + 2(\alpha b - c)j - (k-1)(\sqrt{\alpha^2+1} - 1) = 0,$$
$$L_2': \ 2h + 2(\alpha b - c)j + (k-1)(\sqrt{\alpha^2+1} + 1) = 0). \quad (13)$$

As for the point $T_4(0, +1, 0)$, the boundary of the saddle-node bifurcation is a second-order line

$$L_3': \ 2(b^2 + c^2)j^2 - 2chj + c(1-k)j + h^2 - (1-k)h = 0, \quad (14)$$

which is an ellipse with axes parallel to the axes of the ellipse (10), but shifted relative to the origin along the axis h in the opposite direction. The points of contact of the lines L_1' and L_2' and the ellipse (14) on the plane „field–current“ have coordinates

$$h_1' = (k-1)\frac{(b + \alpha c) + b\sqrt{1+\alpha^2}}{2b\sqrt{1+\alpha^2}}, \ j_1' = \frac{\alpha(k-1)}{2b\sqrt{\alpha^2+1}},$$
$$h_2' = -(k-1)\frac{(b + \alpha c) + b\sqrt{1+\alpha^2}}{2b\sqrt{1+\alpha^2}}, \ j_2' = -\frac{\alpha(k-1)}{2b\sqrt{\alpha^2+1}}.$$

As in the previous case, the boundary of the birth/disappearance of limit cycles for the point $T_3(0, -1, 0)$ is the line

$$L_4': \ -2\alpha h + 2(b + \alpha c)j + \alpha(1-k) = 0. \quad (15)$$

3.3. Additional singular points

The system can have additional singular points in addition to the main singular points $T_{3,4}(0, \mp 1, 0)$ (6), the coordinates of these additional singular points simultaneously turn the right parts of the system to zero. This leads to the algebraic system of equations with respect the coordinates of singular points. To find such singular points, let us first reduce the algebraic system to one equation with respect to the coordinate m_z by replacing variables and obtain

$$A_4 m_z^4 + A_2 m_z^2 + A_0 = 0, \quad (16)$$

where

$$A_4 = b^2 j^2 (k-1)^2,$$
$$A_2 = (k-1)^2(h - cj - bj)(h - cj + bj),$$
$$A_0 = \left[(h - cj)^2 + (k-1)(h - cj) + b^2 j^2\right] \times \left[(h - cj)^2 - (k-1)(h - cj) + b^2 j^2\right].$$

Equation (16) has valid roots if the following condition is met:

$$D = A_2^2 - 4A_0A_4 = (k-1)^2(c^2 j^2 - 2hcj + h^2 + b^2 j^2)^2 \times [(k-1)^2 - 4b^2 j^2] \geq 0 \ (0 \leq m_z^2 \leq 1).$$

Thus, the existence of additional singular points in the system depends on the sign of the multiplier $(1-k)^2 - 4b^2 j^2$ — they may exist in the band between the lines L_0 and L_0' $j \leq |1-k|/(2b)$, but they cannot exist outside this band. Additional conditions for their existence are restrictions on the magnitude of the component modulus m, namely, $0 \leq m_z^2 \leq 1$.

It is easy to determine remaining coordinates m_x and m_y of the additional singular point knowing its coordinate m_z from (6) for example:

$$m_x = bj(1 - m_z^2)m_z \frac{k-1}{b^2 j^2 + (h - cj)^2},$$
$$m_y = \frac{h - cj + \alpha bj - \alpha(k-1)m_x m_z}{m_z(k-1) + m_x(\alpha h - \alpha c j - bj)}.$$

It should be noted that the value $k < 1$ corresponds to a soft magnetic material, whereas the value $k > 1$ corresponds to a hard magnetic material.

4. Numerical results

Point $P_0(h = 0, j = 0)$ (*point 0*)

In this case, the system (6) degenerates to the form

$$\frac{dm_x}{d\tau} = -m_z(k-1)(\alpha m_x m_z + m_y),$$
$$\frac{dm_y}{d\tau} = -m_z(k-1)(\alpha m_y m_z - m_x),$$
$$\frac{dm_z}{d\tau} = -m_z(k-1)(m_z^2 - 1). \quad (17)$$

It can be seen from (17) that the system has a singular line $m_z = 0$ coinciding with the equator of the unit sphere, and two isolated singular points of the focus type with coordinates $(0, 0, \pm 1)$. The foci are unstable in soft magnetic materials $(k < 1)$ and the points are stable on the equator, on the contrary the foci $(0, 0, \pm 1)$ are stable in hard magnetic materials $(k > 1)$ and the singular points are unstable on the equator. Figure 2 shows the hodographs of the end of the normalized magnetization vector for both cases, obtained by numerical solution of the system (6) using the Runge-Kutta method for a three-layer structure based on a soft magnetic material Ta|$Co_{60}Fe_{20}B_{20}$|MgO $(k = 0.892)$ (Figure 2, *a*) and for a three-layer structure based on a hard magnetic material $(k = 3.53)$ (Figure 2, *b*).

Let the initial position of the magnetization vector in a soft magnetic ferromagnetic layer be maintained in a position perpendicular to the plane of the layer and correspond to special points $T_{5,6}(0, 0, \pm 1)$. When the field

and current are switched off, the singular points on the phase portrait of the dynamical system (6) become unstable, and the magnetization vector occupies a new stable position in the plane of the layer at the equator of the unit sphere. This position corresponds to a special line, and is randomly oriented in the plane of the equator, depending on the initial deviation of the vector from the equilibrium position. Any point on the upper and lower hemispheres, located above or below the equator, belongs to a trajectory that begins at the north or south pole of the sphere and ends at some point on the equator. Figure 2, *a* shows the trajectories of transition to a new equilibrium from the upper and lower positions of the magnetization vector.

It should be noted here that although the magnetization vector in the soft magnetic active layer is located in the equatorial plane in the equilibrium state, the type of anisotropy of the active layer material remains the same: the anisotropy field is perpendicular to the layer plane. The equilibrium state of the magnetization vector in the plane is the result of the combined action of the demagnetization field and the anisotropy field.

In the case of a hard magnetic material, the singular points $T_{5,6}(0, 0, \pm 1)$ are stable, and the points that make up the singular line at the equator are unstable. Consequently, the magnetization vector returns from any point of the upper hemisphere to the vertical position corresponding to the north pole of the sphere, and from any point of the lower hemisphere to the position corresponding to the south pole (Figure 2, *b*).

Next, let us consider the cases when h and j are not equal to zero at the same time.

Figure 3 in the center shows a bifurcation diagram based on the results of the analysis of the singular points of the system (6). The dimensional values of the external magnetic field (**H**), in which the memory element is placed, and the density of the charging current passed through a heavy metal bus (**J**) are plotted on the left and lower coordinate axes. The same values normalized by the coefficients from Table 2 for the structure $Ta|Co_{60}Fe_{20}B_{20}|MgO$ are plotted on the right and upper axes. The diagram shows the critical lines $L_{0,1,2,3}$, $L'_{0,1,2,3}$, $P_{1,2}$ and $P'_{1,2}$ dividing the plane into regions of qualitatively equivalent dynamics; some typical points are also plotted *1*–*8* in the upper half-plane of the bifurcation diagram, for which phase portraits of the system on the surface of the unit sphere are constructed. The numbering of the points on the bifurcation diagram corresponds to the numbers of the phase portraits on the sphere. The distribution of points is symmetrical in the lower half-plane because of the symmetry of the dynamical system. The points *1* and *4* correspond to the dynamics of magnetization under the action of spin current without the support of a magnetic field — this case is broadly discussed in modern literature (see, for instance, the review [8]), as it opens promising prospects for simplifying the design of a memory cell. The point *1* is located above the critical line L_0 in the region III. According to the analysis from the previous section, there are only two singular points here, $T_{3,4}(0, \mp 1, 0)$ — an unstable focus at $T_3(0, -1, 0)$ and a degenerate stable node $T_4(0, +1, 0)$. As a result, under the action of the spin current $j > |1 - k|/(2b)$, the magnetization vector will occupy a position coinciding with the direction of the axis OY. The position of the singular points $T_{3,4}(0, \mp 1, 0)$ remains the same when the current structure is affected in the opposite direction, but their type changes, so that the magnetization vector reverses. Thus, the currents from the region of III of the bifurcation diagram are the most effective for switching the direction of magnetization. The magnetization switching takes place in the plane of the layer (and not perpendicular to it, as one might assume from the type of anisotropy of the layers of the structure). Considering that the cell is controlled in pulsed mode, when the current is turned off in the case of a soft magnetic material of the active layer, the magnetization vector will remain in indifferent equilibrium, since the equator of the unit sphere is a special line consisting of stable singular points (see Figure 2, *a*).

Further. The point *3* is located in the region II inside the ellipse L_3. The singular point T_3 is an unstable focus with these values of the control parameters, the point T_4 is a saddle, and the points $T'_{5,6}$ are stable foci. The magnetization vector will take an unpredictable (random) position in the plane of the free layer after switching off the current. The point *2* from the region I corresponds to six special points of the system (6), two of which, $T'_{1,2}$, — saddles (unstable), the third, $T_3(0, -1, 0)$, — unstable focus, the fourth, $T_4(0, +1, 0)$, — stable node, and two stable foci $T'_{5,6}$. Therefore, the magnetization vector can occupy one of three (probable) positions in this parameter range, which makes this situation interesting from the point of view of its use in neural networks. The vector can also take a random position in the plane of the layer when the current is turned off.

The following examples (points *5*–*8*) illustrate how an external magnetic field affects the dynamics of magnetization at a constant current value. The dimensionless value of the current density is 0.18 at point *4* — in this case, the point $T_3(0, -1, 0)$ is an unstable focus, the point $T_4(0, +1, 0)$ is a saddle, and the points $T'_{5,6}$ — stable focus. The magnetization vector can occupy one of two positions $T'_{5,6}$ with a non-zero current, and it again can occupy a random position in the plane of the layer when the current is switched off. A change of the magnitude of the field in its previous direction and at the same value of the current density does not qualitatively change the phase portrait, and therefore the nature of the magnetization dynamics. Let us change the direction of the external field to the opposite (points *6, 7* on the bifurcation diagram) — in this case, the point $T_3(0, -1, 0)$ becomes a saddle, the point $T_4(0, +1, 0)$ — a stable node, the points $T'_{5,6}$ — unstable foci. The magnetization vector will take a stable position in the plane of the layer when the current is turned off.

The upper and lower boundaries of the region I are determined by the values $j = |(1 - k)/(2b)|$ (see above). Thus, for the structure considered here as an example, the dimensionless critical current is $j_{\max} = 0.29$, which in dimensional

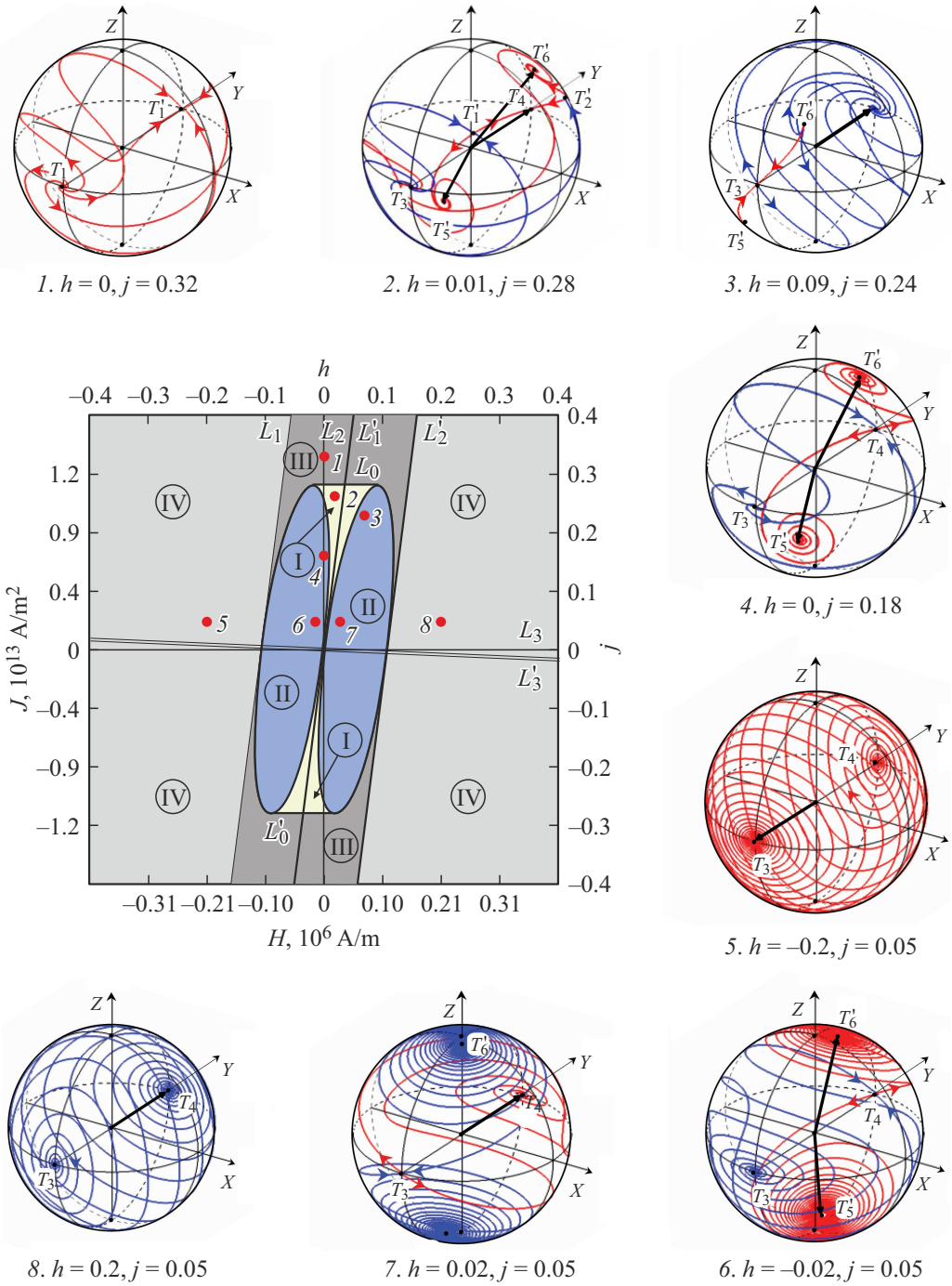

Figure 3. Bifurcation diagram of a dynamical system describing the dynamics of magnetization in an element SOT-MRAM with perpendicular anisotropy for $k = 0.892$, $\alpha = 0.008$. The dynamical system has six singular points in regions I, it has four singular points in regions II, two singular points in the outer regions III and IV, namely $(0, \pm 1, 0)$. The arrow from the origin marks the stable equilibrium position of the magnetization vector.

units corresponds to the values $J_{\max} = 1.18 \cdot 10^{12}$ A/m^2. The dynamical system (6) has four singular points in regions II and III. Two of them are unstable and located on the OY axis (unstable focus and saddle), the other two (two stable foci) are located on the upper and lower hemispheres of the unit sphere. Thus, if the magnetization vector in the model in the absence of an external field and current occupied a position on the equatorial plane, which can be identified with the OY axis, then application a charge current pulse will transfer it to one of the positions T_5, T_6', switching off of the current will return the magnetization vector to the equator plane. Conclusion: it is impossible to write a bit of information into the cell with the values of the control parameters (field and current) from the region I (Figure 3).

Let us estimate the density of the magnetization switching current in the memory cell SOT-MRAM. If at the initial moment the magnetization vector was in the position of indifferent equilibrium $T_3(0, -1, 0)$, then when a pulse of charge (unpolarized) current is applied to the bus of a value above the threshold $j > |(1-k)/(2b)|$, the position $T_3(0, -1, 0)$ loses stability — the equilibrium $T_4(0, +1, 0)$ becomes stable. The magnetization vector rushes to a new equilibrium in the result of small deviation of the magnetization vector from the equilibrium $T_3(0, -1, 0)$ and a magnetization reversal takes place if the duration of the current pulse is sufficient, i.e., a bit of information is written to the cell. We assume that the optimal switching conditions correspond to the case of two equilibrium points (region III in Figure 3). The density of the switching threshold current in this case is approximately $1.15 \cdot 10^{12}\,\mathrm{Am}^{-2}$, i. e. the current value will be 0.1 mA through the cross section of the element with an area of $10 \times 10\,\mathrm{nm}^2$. This value of the control current density is close to the value of the current density for the Z-configuration of the memory cell in operation [5]. However, the configuration considered in this paper has a significant advantage over the configurations described in Ref. [5] — this is the presence of the main singular points $T_{3,4}(0, \pm 1, 0)$, which exist at any values of the control parameters and which can be interpreted as zero and one of the state of the memory cell.

5. Conclusion

In summary, let us list the main results of the study.

1. A system of equations describing the dynamics of the magnetization vector in a SOT-MRAM cell with perpendicular anisotropy of the free layer was constructed.

2. It was analyzed using the methods of the qualitative theory of dynamical systems [9–11]. A bifurcation diagram of the change of dynamic modes was plotted on the plane of the control parameters „field–current“.

3. The control parameters for which the system has six, four, or two equilibrium states were identified. The types of their stability were determined.

4. The critical values of the switching current of the cell were calculated.

5. It was demonstrated that the cell can be switched with a single current at currents above critical values without the support of an external magnetic field.

Funding

The work was funded from the state budget project „Vega-Ct-2023“ „Research and development of methods for creating an element base and software products for high-performance computing systems of the new generation“.

Conflict of interest

The authors declare that they have no conflict of interest.

Appendix
Reduction of the vector equation of LLG to the normal form

Equation (5) can be derived from equation (4) by equivalent transformations.

Let us consider the dimensionless LLG equation

$$\frac{\partial \mathbf{m}}{\partial \tilde{\tau}} = -\mathbf{m} \times \mathbf{f} + \alpha \mathbf{m} \times \frac{\partial \mathbf{m}}{\partial \tilde{\tau}}, \tag{A1}$$

where $\mathbf{f}$ — the effective field taking into account the field associated with the spin-orbit torque $\mathbf{T}_{\mathrm{SOT}}$. In this case

$$\begin{aligned}\mathbf{f} &= \mathbf{h}_{\mathrm{eff}} - bj\mathbf{m} \times \mathbf{e}_y - bj\mathbf{e}_y \\ &= (h + km_x + bjm_z)\mathbf{e}_x - bj\mathbf{e}_y + (-bjm_x - m_z)\mathbf{e}_z.\end{aligned}$$

Step 1. Multiply the equation (A1) vector from the left by the value $\alpha\mathbf{m}$:

$$\alpha\mathbf{m} \times \frac{\partial \mathbf{m}}{\partial \tilde{\tau}} = -\alpha\mathbf{m} \times \mathbf{m} \times \mathbf{f} + \alpha^2 \mathbf{m} \times \mathbf{m} \times \frac{\partial \mathbf{m}}{\partial \tilde{\tau}}.$$

Step 2. Let's use the well-known vector identity $\mathbf{a} \times \mathbf{b} \times \mathbf{c} = \mathbf{b}(\mathbf{a}, \mathbf{c}) - \mathbf{c}(\mathbf{a}, \mathbf{b})$. We will obtain the following

$$\begin{aligned}\alpha\mathbf{m} \times \frac{\partial \mathbf{m}}{\partial \tilde{\tau}} = &-\alpha\mathbf{m}(\mathbf{m}, \mathbf{f}) + \alpha\mathbf{f}(\mathbf{m}, \mathbf{m}) \\ &+ \alpha^2\left(\mathbf{m}, \frac{\partial \mathbf{m}}{\partial \tilde{\tau}}\right) - \alpha^2 \frac{\partial \mathbf{m}}{\partial \tilde{\tau}}(\mathbf{m}, \mathbf{m}).\end{aligned}$$

Thus, taking into account $(\mathbf{m}, \mathbf{m}) = 1$ and

$$\left(\mathbf{m}, \frac{\partial \mathbf{m}}{\partial \tilde{\tau}}\right) = \frac{1}{2} \cdot \frac{\partial (\mathbf{m}, \mathbf{m})}{\partial \tilde{\tau}} = 0,$$

The Gilbert dissipative term has the following form

$$\alpha\mathbf{m} \times \frac{\partial \mathbf{m}}{\partial \tilde{\tau}} = -\alpha\mathbf{m}(\mathbf{m}, \mathbf{f}) + \alpha\mathbf{f} - \alpha^2 \frac{\partial \mathbf{m}}{\partial \tilde{\tau}}.$$

Step 3. Substitute it into the original equation (A1) and transfer the term from the time derivative to the left side. We will obtain the following

$$(1 + \alpha^2) \frac{\partial \mathbf{m}}{\partial \tilde{\tau}} = -\mathbf{m} \times \mathbf{f} - \alpha\mathbf{m}(\mathbf{m}, \mathbf{f}) + \alpha\mathbf{f}.$$

Step 4. Renormalize the time $\tilde{\tau}$ obtaining the following equation

$$\frac{\partial \mathbf{m}}{\partial \tau} = -\mathbf{m} \times \mathbf{f}_{\mathrm{eff}} + \alpha\mathbf{f}_{\mathrm{eff}}(\mathbf{m}, \mathbf{m}) - \alpha\mathbf{m}(\mathbf{m}, \mathbf{f}_{\mathrm{eff}}). \tag{A2}$$

This implies the equivalence of equations (A1) and (A2), i.e. the conditions of applicability of equation (A2) are the same as equations (A1).

References

[1] S.A. Wolf, D.D. Awschalom, R.A. Buhrman, J.M. Daughton, S. von Molnar, M.L. Roukes, A.Y. Chtchelkanova, D.M. Treger. Sci. **294**, *5546*, 1488 (2001).
[2] S.D. Bader, S.S.P. Parkin. Annu. Rev. Condens. Matter Phys. **1**, 71 (2010).
[3] A. Brataas, A.D. Kent, H. Ohno. Nature Mater. **11**, *5*, 372 (2012).
[4] C. Song, R. Zhang, L. Liao, Y. Zhou, X. Zhou, R. Chen, Y. You, X. Chen, F. Pan. Progr. Mater. Sci. **118**, *5*, 100761 (2021).
[5] S. Fukami, T. Anekawa, C. Zhang, H. Ohno. Nature Nanotechnol. **11**, *7*, 621 (2016).
[6] J.M. Shaw, H.T. Nembach, M. Weiler, T.J. Silva, M. Schoen, J.Z. Sun, D.C. Worledge. IEEE Magn. Lett. **6**, 3500404 (2015).
[7] D. Jhajhria, D.K. Pandya, S. Chaudhary. AIP Conf. Proceed. **1953**, *1*, 120034 (2018).
[8] H. Wu, J. Zhang, B. Cui, S.A. Razavi, X. Che, Q. Pan, D. Wu, G. Yu, X. Han, K.L. Wang. Mater. Futures *1*, *2*, 022201 (2022).
[9] J. Guckenheimer, P. Holmes. Nonlinear Oscillations, Dynamical Systems, and Bifurcations of Vector Fields. Appl. Math. Sci. **42**, Springer (1983).
[10] N.N. Bautin, E.A. Leontovich. Methody i priemy kachestvennogo issledovania dinamicheskikh sistem na ploskosti. Nauka, M. (1990). 488 s. (in Russian).
[11] A.A. Andronov, E.A. Leontovich, I.I. Gordon, A.G. Mayer. Kachestvennaya teoriya dinamicheskih sistem vtorogo poryadka. Nauka, M. (1966). 568 s. (in Russian).
[12] R. Skomski. Simple Models of Magnetism. Oxford University Press, N.Y. (2008). 335 p.
[13] N.V. Ostrovskaya, V.A. Skidanov, Yu.A. Yusipova. Matematicheskaya model' yachejki SOT-MRAM cilindricheskoj formy. V sb.: Problemy razrabotki perspektivnykh mikro- i nanoelektronnykh sistem (MES) / Pod red. A.L. Stempkovsky. Vyp. IV. M.,Zelenograd (2022). S. 142–148. (in Russian). https://doi.org/10.31114/2078-7707-2022-4-142-148

Translated by A.Akhtyamov